JGP Journal of General Physiology

ARTICLE

The epithelial potassium channel Kir7.1 is stimulated by progesterone

Ida Björkgren, Sarah Mendoza*, Dong Hwa Chung*, Monika Haoui*, Natalie True Petersen, and Polina V. Lishko

The choroid plexus (CP) epithelium secretes cerebrospinal fluid and plays an important role in healthy homeostasis of the brain. CP function can be influenced by sex steroid hormones; however, the precise molecular mechanism of such regulation is not well understood. Here, using whole-cell patch-clamp recordings from male and female murine CP cells, we show that application of progesterone resulted in specific and strong potentiation of the inwardly rectifying potassium channel Kir7.1, an essential protein that is expressed in CP and is required for survival. The potentiation was progesterone specific and independent of other known progesterone receptors expressed in CP. This effect was recapitulated with recombinant Kir7.1, as well as with endogenous Kir7.1 expressed in the retinal pigment epithelium. Current-clamp studies further showed a progesterone-induced hyperpolarization of CP cells. Our results provide evidence of a progesterone-driven control of tissues in which Kir7.1 is present.

Introduction

Situated in the ventricles of the brain, the choroid plexus (CP) constitutes an important barrier between the peripheral blood plasma and the brain. The CP consists of a layer of cuboidal epithelial cells that are responsible for producing cerebrospinal fluid (CSF; Damkier et al., 2013). In addition to its function as a mechanical buffer, secretion of CSF also provides the nutrients and hormones needed for neurogenesis while, at the same time, removing waste products from the brain (Lun et al., 2015). Tight junctions in the CP epithelium form a barrier between the blood plasma and the CSF, which allow channels and transporters in the CP to establish a highly regulated concentration gradient of ions between the two fluids (Damkier et al., 2013). Therefore, identification of the molecular regulators of CP ion channels is essential to better understand the mechanism behind the healthy ion homeostasis and CP function. One such potential regulator is the steroid hormone progesterone (P4), the levels of which were shown to correlate with ventricular size during the female menstrual cycle (Hagemann et al., 2011) and pregnancy (Oatridge et al., 2002). Interestingly, the expression of the conventional genomic progesterone receptor in CP, as well as other steroid receptors (Table 1), is almost negligible, while the tissue retains a response to P4-induced regulation (Kelley and Mermelstein, 2011; Luoma et al., 2011). Additionally, P4 has been shown to exert a neuroprotective role during brain trauma (Pettus et al., 2005; Stein and Wright, 2010; Deutsch et al., 2013). Intramuscular or intravenous injections of micromolar concentrations of P4 have been shown to alleviate traumatic brain injury (TBI) outcomes and decrease brain edema (Pan et al., 2019), yet the molecular mechanism behind this effect is still unknown. Since P4 is known to regulate cationic channels through nongenomic steroid signaling (Lösel and Wehling, 2003; Miller et al., 2016), we explored whether P4 could modulate CP ion channels in a similar manner. To determine nongenomic signaling events, direct patch-clamp experiments were performed on primary cultures of murine CP cells isolated from the lateral ventricles. These experiments revealed that the inwardly rectifying potassium channel Kir7.1, localized to the luminal side of the CP epithelium, is the major ion channel in CP potentiated by P4 via a G protein–coupled receptor-independent mechanism. Kir7.1 is vital for mammalian physiology, as mice deficient in Kir7.1 die shortly after birth (Yin et al., 2018). The potentiation of Kir7.1 by P4 was recapitulated using recombinantly expressed Kir7.1 in HEK293 cells. Similarly, we found that P4 potentiated the endogenous Kir7.1 expressed in the retinal pigment epithelium (RPE; Shimura et al., 2001), another epithelial tissue with similar ion channel expression as the CP. Our results point to a novel unexpected regulation of Kir7.1 by the steroid hormone P4 in two tissues, CP and RPE.

Materials and methods

Ethics statement

The C57BL/6N (Charles River) mice and the *Abhd2* knockout mice of similar background were kept at the Animal Facility of

Department of Molecular and Cell Biology, University of California, Berkeley, Berkeley, CA.

*S. Mendoza, D.H. Chung, and M. Haoui contributed equally to this paper; Correspondence to Polina V. Lishko: lishko@berkeley.edu.

Table 1. **Expression of steroid receptors in the CP of adult female and male wild-type mice, analyzed by mRNA sequencing**

Gene	Protein	Female (FPKM)	Male (FPKM)	P value (male vs. female)
Ar	Androgen receptor	0.0395	0.04	0.94
Esr1	Estrogen receptor 1 (α)	0.06	0.03	0.24
Esr2	Estrogen receptor 2 (β)	0.098	0.13	0.49
Pgr	Progesterone receptor	0.008	0.014	0.74
Paqr7	Membrane progesterone receptor α	5.09	4.96	0.84
Paqr8	Membrane progesterone receptor β	1.60	1.53	0.65
Paqr5	Membrane progesterone receptor γ	12.90	15.77	0.0023**
Paqr6	Membrane progesterone receptor δ	1.85	1.18	0.044*
Paqr9	Membrane progesterone receptor ε	9.86	7.92	0.0013**
Pgrmc1	Progesterone receptor membrane component 1	301.29	310.57	0.43
Pgrmc2	Progesterone receptor membrane component 2	54.90	59.81	0.062
Abhd2	Abhydrolase domain–containing protein 2	351.53	300.73	0.0070**

n = 3 for each sex. Statistical significance is indicated as follows: *, P ≤ 0.05; **, P ≤ 0.01.

the University of California, Berkeley, in a room with controlled light (14 h light, 10 h darkness) and temperature (23 ± 0.5°C). The mice were fed a standard chow diet (LabDiet 5053; PicoLab Rodent diet 20) and hyperchlorinated water ad libitum. All experiments were performed in accordance with National Institutes of Health guidelines for animal research and approved by the University of California, Berkeley Animal Care and Use Committee (AUP 2015-07-7742), with every effort made to minimize suffering for the animals. A thorough description of how the *Abhd2* full knockout mouse line was generated is provided elsewhere (Björkgren et al., 2019 *Preprint*).

mRNA library preparation and sequencing

For gene expression analyses of the CP, the lateral CPs from three adult male and three adult female of either $Abhd2^{+/+}$ or $Abhd2^{-/-}$ genotype were dissected out and snap frozen. The animals were euthanized by CO_2 followed by cervical dislocation. This procedure was performed in the morning when the females were in proestrus. mRNA isolation was performed using the Quick-RNA Microprep Kit (Zymo Research; R1050) according to the manufacturer's instructions. The mRNA samples were processed for sequencing at QB3 Vincent J. Coates Genomics Sequencing Laboratory, University of California, Berkeley. CP mRNA was enriched for using Oligo dT beads from the Invitrogen Dynabeads mRNA Direct kit (61005). Subsequent library preparation steps of fragmentation, adapter ligation, and cDNA synthesis were done on the enriched mRNA using the KAPA RNA HyperPrep kit (Roche; KK8540). Truncated universal stub adapters were used for ligation, and indexed primers were used during PCR amplification to complete the adapters and to enrich the libraries for adapter-ligated fragments. Samples were checked for quality on an AATI (now Agilent) Fragment Analyzer. Libraries were then quantified using qPCR on a Bio-Rad CFX Connect to measure molarity of only sequenceable molecules using the Kapa Biosystems Universal Illumina quant kit (KK4824), pooled equimolar, clustered at 3 nM with 2% PhiX v3 control library spike-in, and sequenced as a 100-bp paired-end run on an Illumina HiSeq 4000. BCL files were then converted to fastq format and demultiplexed using the innate bcl2fastq v1.19 software.

Data analysis

The sequencing results were analyzed by Novogene. Reference genome and gene model annotation files were downloaded from the genome website browser (NCBI/UCSC/Ensembl) directly. Indexes of the reference genome was built using STAR and paired-end clean reads were aligned to the reference genome using STAR (v2.5) and the method of maximal mappable prefix. HTSeq v0.6.1 was used to count the read numbers mapped of each gene. Thereafter, fragments per kilobase of exon model per million reads mapped (FPKM) of each gene was calculated based on the length of the gene and reads count mapped to this gene (Mortazavi et al., 2008). Differential expression analysis between the four groups ($Abhd2^{+/+}$ and $Abhd2^{-/-}$ male versus $Abhd2^{+/+}$ and $Abhd2^{-/-}$ female, three biological replicates per condition) was performed using the DESeq2 R package (2_1.6.3). The resulting P values were adjusted using Benjamini and Hochberg's approach for controlling the false discovery rate. Genes with an adjusted P value < 0.05, found by DESeq2, were assigned as differentially expressed. The data discussed in this publication have been deposited in NCBI's Gene Expression Omnibus (Edgar et al., 2002) and are accessible through GEO Series accession number GSE181594.

Lateral CP cell culture

The lateral CPs from two animals of similar age were used for each cell culture. Animals were euthanized by CO_2 followed by cervical dislocation, and the sheets of CP epithelial cells (CPECs) were dissected out from the lateral ventricles into 37°C growth media (high-glucose Dulbecco's modified Eagle's medium with L-glutamine [Thermo Fisher Scientific; 11965092], 10% FBS [X&Y Cell Culture; FBS-500-HI], and 1% Penstrep [Thermo Fisher Scientific; 15140–122]), after which the CPs were transferred into 37°C Dulbecco's PBS (DPBS) without Ca^+ and Mg^+ (Thermo Fisher Scientific; 14190144). Enzymatic dissociation of cells from the CP sheets was performed as previously described (Johnson et al., 2018), with some minor modifications. The CP sheets were broken up by incubation with Pronase (0.1 mg/ml in DPBS; Sigma; 10165921001) at 37°C for 30 min. The reaction was inhibited by adding a 5× volume of DPBS after which the cells were allowed to sediment. The cell pellet was further dissociated by trituration in 37°C TrypLE Express (Thermo Fisher Scientific;

12605010). After the cell clusters had sedimented, the supernatant was transferred to a 5× volume of fresh growth media. The trituration was repeated five times until only minor cell aggregates remained. The CPECs were washed in growth media by centrifugation at 800 ×*g* for 5 min, resuspended in fresh growth media, and plated on poly-D-lysine and laminin (Cell Applications; 127)–coated 5-mm glass coverslip in a 96-well plate. The cells were allowed to attach to the coverslip for 3 h at 37°C and 5% CO_2 before electrophysiology measurements.

RPE cell culture

RPE cells from two animals of similar age were used for each cell culture. The eyes were processed as previously described (Shang et al., 2018). In brief, the eyes were isolated and incubated in 2% Dispase II (Sigma; D4693) in high-glucose Dulbecco's modified Eagle's medium, without glutamine or pyruvate (Thermo Fisher Scientific; 11960044), for 45 min at 37°C and 5% CO_2 to allow the eye tissue to soften. Afterward, the cornea, iris, and lens capsule were removed, and the remaining eye tissue was incubated in RPE culture media (10% Charcoal-Stripped FBS [R&D Systems; S11650], 1% Penstrep, 2.5 mM L-glutamine [GIBCO BRL; 25030–81], and 1X MEM nonessential amino acids [Thermo Fisher Scientific; 11140050]) for 20 min at 37°C and 5% CO_2 to allow the neural retina to detach from the RPE. The RPE sheets were then manually dissected out and placed in an Eppendorf tube where the cells were dissociated from each other by pipetting up and down ∼40 times. The single-cell suspension was plated on laminin (GIBCO BRL; 23017–015)–coated 6.5-mm, 0.4-µm-pore Polyester Transwell membranes (Costar; 3470) in RPE culture media and incubated at 37°C and 5% CO_2 for 24 h before being used for electrophysiology measurements.

Cloning of Kir7.1 and expression in HEK293 cells

The complete open reading frame of *Kcnj13* (the gene encoding Kir7.1) was amplified from a cDNA library, generated by standard procedures from a C57BL/6N male murine small intestine, an organ known to express high levels of *Kcnj13*. Primers used for the amplification bound to the untranslated region of the gene (in capital letters) with added restriction sites for SacI and SalI (Kir7.1 forward, SacI: 5′-ataagagctcCACAAAGGAACCGAGAA ACAC-3′; Kir7.1 reverse, SalI: 5′-ataagtcgacGGACGGTGTAGATG AGTCTTA-3′). After restriction digest of the sequence-confirmed full-length *Kcnj13* and the mammalian expression vector pIRES2-EGFP (Clonetech; 6029–1) by standard procedures, *Kcnj13* was inserted into the vector using the Quick Ligation Kit (New England BioLabs; M2200) according to the manufacturer's instructions. For recombinant expression, cells of the human embryonic kidney cell line (ATCC; HEK293, CRL-1573) were plated on collagen (Roche; 11179179001)–coated coverslips and transfected using Lipofectamine 2000 reagent (Life Technologies; 11668027) according to the manufacturer's recommendation. Overexpression was verified by the presence of Kir7.1 in immunocytochemical staining and Western blot analysis as mentioned below. The EGFP of the pIRES2-EGFP vector was used to visualize the transfected cells for whole-cell patch-clamp experiments.

Immunohistochemistry and immunocytochemistry

For staining of mouse brain sections, C57BL/6N, *Abhd2*$^{+/+}$, and *Abhd2*$^{-/-}$ adult male mice were euthanized by perfusion with 4% paraformaldehyde (PFA; Electron Microscopy Sciences; 15714S) after which the brains were dissected out, placed in a sucrose gradient, and frozen in Tissue-Tek O.C.T. compound (Sakura; 4583). The brains were sectioned using a cryotome into 8-µm-thick coronal sections. For Kir7.1 staining, the sections were permeated by incubation with 0.5% Triton X-100 (Fisher BioReagents; BP151-100) for 15 min. For the detection of α/β hydrolase domain–containing protein 2 (ABHD2), antigen retrieval was performed by incubation with 1% SDS (Sigma; L4509-100G) for 5 min. Thereafter, the sections were washed three times in PBS, blocked with 5% BSA (Sigma; A9647) for 1 h at room temperature, and incubated with primary antibody in PBS supplemented with 1% BSA overnight at 4°C. After washing three times in PBS, the sections were incubated with secondary antibody for 1 h, washed three times in PBS, and mounted.

For the detection of both ABHD2 and Kir7.1 in CPECs isolated from *Abhd2*$^{+/+}$ and *Abhd2*$^{-/-}$ mice, the cells were fixed with 2% PFA in PBS for 15 min and washed three times with PBS followed by antigen retrieval for 5 min using 0.75% SDS. For blocking, the cells were incubated overnight in 3% BSA and 0.1% Saponin (Sigma; 47036-50G-F) in PBS at +4°C, followed by overnight incubation with the primary antibody in blocking solution at +4°C. After washing three times in 0.1% saponin/PBS solution, the cells were incubated with secondary antibody in PBS supplemented with 1% BSA and 0.1% saponin for 1 h, washed three times in 0.1% saponin/PBS solution, and mounted. For detection of Kir7.1 in HEK293 cells (transfected as previously mentioned and cultured overnight on poly-D-lysine (Millipore; P1024) coated coverslips), the cells were fixed with 4% PFA in PBS for 10 min, permeated, stained, and mounted according to the protocol for Kir7.1 staining of brain sections.

For detection of Kir7.1 in cultured RPE cells (isolated and cultured overnight on poly-D-lysine– and laminin-coated coverslips), cells were fixed with 2% PFA in PBS for 15 min and washed three times with PBS. Next, permeabilization and blocking of the cells were performed simultaneously by 1-h incubation in blocking solution (1% BSA and 0.1% saponin in PBS). The cells were then incubated with the primary antibody in the blocking solution overnight at 4°C. After washing three times in 0.1% saponin/PBS, the cells were incubated with secondary antibody for 1 h, washed three times in 0.1% saponin/PBS solution, and mounted.

The following primary antibodies were used: rabbit polyclonal anti-ABHD2 (Proteintech Group; 1:300, 14039–1-AP) and mouse monoclonal anti-Kir7.1 (Santa Cruz Biotechnology; 1:300, sc-398810). The following secondary antibodies conjugated with different fluorescent dyes were used: Dylight 488–conjugated goat anti-rabbit IgG (1:2,000; Molecular Probes; A11008; Jackson ImmunoResearch; 111–485-144) and Cy5-conjugated donkey anti-mouse (Jackson ImmunoResearch; 1:2,000, 715–175-150). For mounting, we used ProLong Gold antifade reagent with DAPI (Invitrogen; P36935). The cells were visualized with an inverse microscope (Olympus; IX71) equipped with lumencor light engine (SPECTRAX; 6-LCR-SA) while the brain sections were

visualized using a confocal laser scanning microscopy (Olympus; Fluoview FV1000).

In situ hybridization (ISH)

Lateral CP slices, isolated as described above, were used for ISH. RNA was extracted from the murine ovary using a Qiagen RNAeasy mini kit followed by cDNA synthesis with a Phusion RT-PCR kit (Finnzymes). The specific translated region of *Abhd2* was amplified using the following primers: (forward, 5′-GTC GGATGGTGCCACTTC-3′; reverse, 5′-CCTCCATCTGCTCCGTGT-3′) and subcloned into a vector containing Sp6/T7 promoters (Promega). Single-strand digoxigenin-labeled RNA probes were synthesized (Roche), and color ISH was performed as in Ishii et al. (2004). A sense probe was used as a negative control.

Western blotting

To detect Kir7.1 in HEK293 cells transfected with the pIRES2-EGFP/Kir7.1 construct, the cells were cultured for 24 h after transfection and harvested by standard procedures. The samples were analyzed by Western blotting using the mouse monoclonal antibody against Kir7.1 (1:10,000 dilution) and a peroxidase-conjugated goat anti-mouse secondary antibody (EMD-Millipore; 1:15,000 dilution, AP181P). To ensure equal sample loading, the membrane was stripped by incubation with OneMinute Plus Strip (GM Biosciences; GM6011) according to the manufacturer's instructions. Thereafter, the membrane was rehybridized with mouse monoclonal anti-actin antibody (Abcam; 1:5,000 dilution, ab3280-500) and peroxidase-conjugated goat anti-mouse secondary antibody (1:15,000 dilution).

Reagents for electrophysiology

$KMeSO_3$ was purchased from Alfa Aesar (39505), P4 from Millipore (5341), and VU590 (7,13-bis[(4-nitrophenyl)methyl]-1,4,10-trioxa-7,13-diazacyclopentadecane) dihydrochloride from Fisher (389110). All other compounds were from Sigma. Testosterone (Sigma; T1500) was purchased in accordance with the controlled substance protocol CSUA #123 approved by the University of California, Berkeley, Office of Environment, Health & Safety. For patch-clamp measurements, all bath solutions contained a concentration of 1:1,000 EtOH and DMSO, the solvents used to dissolve the steroid hormones and the antagonist VU590, respectively.

Electrophysiology

CPECs and HEK293 cells, plated on 5-mm glass coverslips, were placed in a perfusion chamber (Warner Instruments; RC-24E), and RPE cells plated on Transwell membranes were placed in an open bath recording chamber (Warner Instruments; RC22) and secured by a slice anchor (Warner Instruments; SHD-22L/15) for electrophysiological measurements at ambient temperatures. Data were acquired using Clampex 10.5 software (Molecular Devices), which controlled an AXOPATCH 200B amplifier and an AxonTM Digidata 1550A digitizer (both from Molecular Devices) with an integrated Humbug noise eliminator. Data were not corrected for liquid junction potential changes. Gigaohm seals were established in dissection media (in mM: 140 NaCl, 15 HEPES, 15 d-glucose, 5 KCl, 1 $CaCl_2$, and 1 $MgCl_2$, [pH 7.3 adjusted with NaOH, 310 mOsm/liter]). The patch pipette was filled with either a Cs^+- or a K^+-based solution (in mM: 130 $CsMeSO_3$ or $KMeSO_3$, 20 HEPES, 5 BAPTA (1,2-bis(o-aminophenoxy)ethane-*N*,*N*,*N*′,*N*′-tetraacetic acid), and 1 $MgCl_2$, [pH 7.3 adjusted with CsOH or KOH, 295 mOsm/liter]) and had a resistance of 3–6 MΩ. For measurements of the difference in monovalent currents, the bath solutions contained, in mM: 43 HEPES, 1 $MgCl_2$, and one of the following: 130 $CsMeSO_3$, 130 $KMeSO_3$, 130 RbCl, or 130 $NaMeSO_3$ [pH 7.3, 310 mOsm/liter]). All buffers, including those containing steroid hormones, were applied under constant perfusion. The Kir7.1 antagonist VU590 (100 µM), in combination with P4, was applied directly to the bath solution. To block G-protein signaling, 1 mM guanosine 5′-O-(2-thiodiphosphate; GDPβS) was applied to the K^+-based pipette solution. Measurements were performed at 10 kHz and filtered at 1 kHz. Cells were stimulated every 5 s by voltage ramps from −80 mV to +80 mV with a holding potential of 0 mV or by 500-ms voltage steps from −120 mV to +40 mV in 20 mV increments with a holding potential of −40 mV. Access resistance and membrane capacitance were between 4 and 10 MΩ and 33 ± 1.09 pF for CPECs, 7–13 MΩ and 19.3 ± 1.08 pF for HEK293 cells, and 10.5–14 MΩ and 12.7 ± 2.17 pF for RPE cells. Membrane capacitance served as a proxy for the cell surface area and used for normalization of current amplitudes (i.e., current density). Capacitance artifacts were graphically removed in OriginPro 8.6 (OriginLab). For current-clamp measurements, the pipette solution contained (in mM) 40 NaCl, 100 $KMeSO_3$, 20 HEPES, 1 BAPTA, 5 Mg-ATP, and 0.5 Na-GTP (pH 7.2 was adjusted with KOH before adding the ATP and GTP stocks, 295 mOsm/liter). The bath solution for current clamp contained (in mM) 140 NaCl, 5 $KMeSO_3$, 1 $MgCl_2$, 20 HEPES, and 10 d-glucose (pH 7.3 adjusted with NaOH, 310 mOsm/liter). Measurements were performed at 10 kHz and filtered at 10 kHz under a gap-free protocol with a 0 pA input signal.

Statistical analysis

For statistical analyses of the activation and inhibition of Kir7.1 by different steroid hormones and the antagonist VU590, in measurements from CPECs, HEK293, and RPE cells, Clampfit 10.3 (Molecular Devices) and GraphPad Prism 5 (GraphPad Software) software was used. Unpaired and paired *t* test were used to determine statistical significance, assigning $P \leq 0.05$ as the limit. All results are shown with SEM.

Online supplemental material

Fig. S1 shows the relative gene expression of the lateral CPs isolated from *Abhd2*$^{+/+}$ and *Abhd2*$^{-/-}$ male and female mice. Fig. S2 shows expression of *Abhd2* in murine CPs. Fig. S3 shows a summary of cumulative current densities recorded during the study and the presence of I_{TRPM3} in CPEC. Data S1 lists the genes expressed in the lateral CPs from wild-type and *Abhd2*$^{-/-}$ male and female mice.

Results

Progesterone potentiates the activity of the inwardly rectifying potassium channel Kir7.1 in CPECs

To study the nongenomic effect of steroid hormones on CP ion conductance, whole-cell patch-clamp experiments were

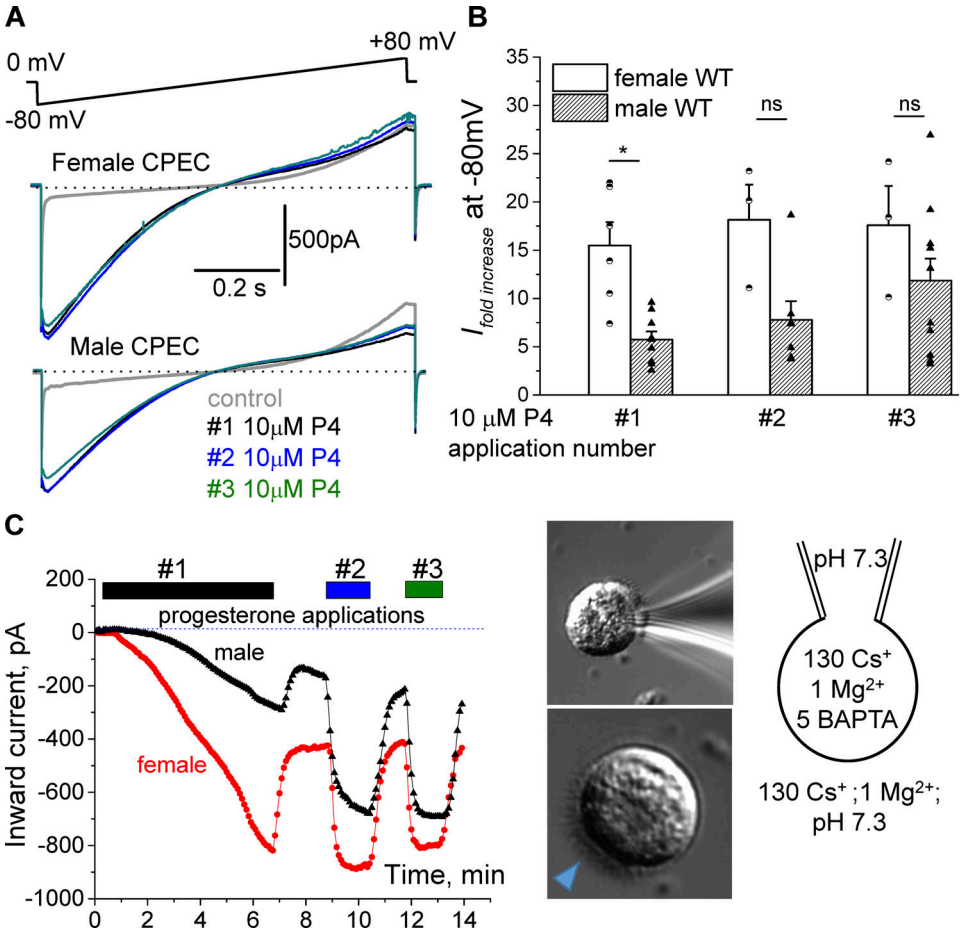

Figure 1. **Potentiation of an inwardly rectifying ion conductance by progesterone in murine CPECs.** Whole-cell recordings from both male and female CPECs show a significant potentiation of an inwardly rectifying ion current upon exposure to 10 μM P4 applied via bath solution. **(A)** Representative traces from isolated lateral CPECs elicited in response to a voltage ramp, as indicated. P4 was administered three times with subsequent washout between readministrations. **(B)** Average fold increase of the inward current recorded at −80 mV from 6 female and 14 male CPECs after subsequent P4 applications, recorded from ramps shown in A. Statistical significance was calculated using the paired *t* test, and the significance of changes is indicated as follows: *, P ≤ 0.05. **(C)** Representative inward current amplitudes obtained at −80 mV from the experiments shown in A and plotted against time show a prolonged response to P4 in both male and female CPECs. The time of applications of 10 μM P4 to the bath solution is indicated by bars above. Bottom right: A differential interference contrast image of a typical CPEC with brush border indicated by the arrowhead. Top right: CPECs attached to a recording pipette. Cartoon depicts ion composition of the pipette and bath solutions. Data are means ± SEM.

performed on CPECs isolated from the murine lateral ventricle. To avoid possible changes in gene expression during prolonged cell culture, all analyses were performed on the same day of tissue collection, within 3–5 h of cell extraction. When the cells were placed in a bath solution containing Cs^+ and Mg^{2+}, a mostly outward current with a small inward component was observed in response to the voltage ramp from −80 mV to +80 mV applied from a holding potential of 0 mV (Fig. 1 A). This inward current was further significantly potentiated by exposure to P4 with a 15.5 ± 2.4-fold and 5.7 ± 0.8-fold increase in cells isolated from female and male CP, respectively (Fig. 1, A and B), developing a strong inward rectification. Interestingly, while the initial response to P4 application was statistically stronger in females, repetitive P4 applications increased the current fold change of male CPECs from the initial 5.7 ± 0.8-fold for the first application to 7.8 ± 1.9-fold for the second and eventually to 11.9 ± 2.3-fold for the third application of P4 (Fig. 1 B). The female CPECs still retained stronger response to P4 for the second (18.2 ± 3.6-fold), as well as for the third (17.6 ± 4.1-fold), applications of this steroid. The cellular response to P4 was also initially slow and required almost 6 min to achieve saturation. However, after subsequent washout and readministrations, the response was almost immediate, with only a slight desensitization of the current (Fig. 1 C). The initial slow activation component was similar among females and males, with average activation kinetics of 4.8 ± 1.3 min for females and 4.5 ± 0.9 min for males (data from three independent experiments).

To determine the ion channel responsible for the observed current, we analyzed mRNA expression data from adult murine CPs. Interestingly, one of the most abundantly expressed ion channels in CPECs is the inwardly rectifying potassium channel Kir7.1 (encoded by *Kcnj13*; Fig. S1 A, Table 2, and Data S1), which is also the only potassium channel that conducts Cs ions and is not blocked by them (Krapivinsky et al., 1998). To test the hypothesis that P4 activates Kir7.1, the Kir7.1/K_{ir}1.1–specific antagonist VU590 was used. VU590 significantly reduced the

Table 2. **Expression of the potassium voltage-gated channel subfamily J (*KCNJ*) in the mouse CP, determined by mRNA sequencing**

Gene	Protein	Female (FPKM)	Male (FPKM)	P value (male vs. female)
Kcnj1	Kir1.1	0	0	NA
Kcnj2	Kir2.1	0.14	0.08	0.255
Kcnj3	Kir3.1	0.002	0.06	0.070
Kcnj4	Kir2.3	0.19	0.18	0.920
Kcnj5	Kir3.4	0.002	0	0.701
Kcnj6	Kir3.2	0	0.01	0.570
Kcnj8	Kir6.1	0.81	0.55	0.279
Kcnj9	Kir3.3	0.03	0.18	0.039*
Kcnj10	Kir4.1	0.61	0.77	0.726
Kcnj11	Kir6.2	0.82	0.76	0.967
Kcnj12	Kir2.2	0.08	0.12	0.686
Kcnj13	Kir7.1	195.13	198.09	0.724
Kcnj14	Kir2.4	0.008	0	0.701
Kcnj15	Kir4.2	0.009	0.02	0.732
Kcnj16	Kir5.1	0.08	0.03	0.271

n = 3 for each sex. Statistical significance is indicated as follows: *, P ≤ 0.05.

inward current and further prevented P4 to potentiate it (Fig. 2 A). Since the expression of *Kcnj1* (encoding Kir1.1) is not detected in CPECs (Table 2 and Data S1), and given the presence of Cs^+ in the recording pipette that should inactivate any potassium channels except Kir7.1, it is highly likely that the observed reduction in current is caused by blocking the activity of Kir7.1. Furthermore, Kir7.1 was detected via immunohistochemical staining in the apical membrane of the murine CP and was also present after lateral CP cell isolation and culture (Fig. 2, B–D). Kir7.1 has a signature ion selectivity with the following order of preference $Rb^+>>Cs^+>K^+>>Na^+$ (Shimura et al., 2001), which was indeed observed in our CPEC recordings, as is evident from representative I-V curves and current density profiles (Fig. 2, E–G). Since Kir7.1 mainly conducts potassium ions in its native state, further experiments were performed using bath and pipette solutions where Cs^+ was replaced with K^+. In addition, 100 µM VU590 was applied at the end of each recording to confirm that the measured potentiated current was not a by-product of a leak current.

Progesterone-specific regulation of Kir7.1 activity

By measuring Kir7.1 potentiation with different concentrations of P4 the half maximal effective concentration for P4 was determined to be 7.02 ± 2.3 µM, with the maximal effective concentration reached ∼50 µM (Fig. 3, A and B). To test whether other steroid hormones are able to increase the activity of Kir7.1, CPECs were stimulated with 10 µM testosterone, estradiol, pregnenolone sulfate (PS) and the synthetic progestin levonorgestrel (Fig. 3, C and D). Surprisingly, none of these steroids were able to significantly change the activity of Kir7.1 (Fig. 3, C and D), although the addition of 10 µM P4 at the end of each experiment still caused a 3.08 ± 0.20-fold increase in the inward current at −80 mV (Fig. 3 D). The results indicate that P4 activation of Kir7.1 is specific for this steroid. The significance of P4 activation was also analyzed by the current-clamp method, where the solutions used had an ion concentration and osmolarity comparable to that of CSF and the intracellular environment of CPECs. To measure the native membrane potential of CPECs, no current was applied to the cells, and the average initial V_m measured was −57.2 ± 4.6 mV (n = 3; Fig. 3 E). Under such conditions, the application of 10 µM P4 caused hyperpolarization of the cells, with an average decrease in membrane potential of 9.13 ± 3.56 mV (Fig. 3, E and F). Similar to the whole-cell patch-clamp recordings, applying 100 µM of the antagonist VU590 caused a significant inhibition of Kir7.1 conductance, which led to depolarization of the cell, with a significant increase in membrane potential of 29.95 ± 6.51 mV, even in the presence of P4 (Fig. 3 E).

Secondary messengers are not required for the potentiation of Kir7.1 activity by progesterone

The CP epithelium contains several membrane-bound P4 receptors that could potentially mediate the cell response to P4. Interestingly, we found that the recently characterized P4 receptor ABHD2 (Miller et al., 2016) is also highly expressed in the CP (Figs. S1 and S2 and Table 1) and cultured CPECs (Fig. 4). ABHD2 has been shown to regulate ion channel activation in human sperm cells by breaking down the endocannabinoid 2-arachidonoylglycerol in the cell membrane (Miller et al., 2016). However, CPECs isolated from global *Abhd2* knockout mice that were generated in our laboratory (Björkgren et al., 2019 *Preprint*) showed activation of Kir7.1 similar to that of cells from wild-type animals (Fig. 4, E and F), thus negating any possible effect of the receptor on Kir7.1 activation. However, CPECs isolated from *Abhd2* knockout female and male mice showed an altered Kir7.1 slow activation component in response to P4 stimulation, with faster activation kinetics of 2.5 ± 0.43 min for females and 1.96 ± 0.36 min for males (data from six to nine independent experiments). The kinetics is significantly faster than the activation kinetics shown by wild-type littermates, with 4.8 ± 1.3 min for wild-type females and 4.5 ± 0.9 min for wild-type males (n = 3). While it is unlikely that ABHD2 is required for Kir7.1 activation by P4, it is possible that its presence changes the bioactive lipid landscape of the cells and alters the channel activation.

To further validate a direct interaction between P4 and Kir7.1, the full-length mRNA sequence of murine *Kcnj13* was cloned into an expression vector and subsequently expressed in HEK293 cells. The cells do not display any endogenous expression of the channel, but, as was demonstrated in a previous study (Carrington et al., 2018), the products of the transfected construct were glycosylated and transported to the cell membrane, as shown by Western blot and immunocytochemistry (Fig. 5, A–D). Whole-cell patch-clamp recordings of the transfected HEK293 cells show a similar potentiation of $I_{Kir7.1}$ after applying 10 µM P4 to the bath solution (Fig. 5, A and E; and Fig. S3 A), and the fast activation of Kir7.1 by P4 in HEK293 cells resembled the activation of CPECs upon second and third P4 application.

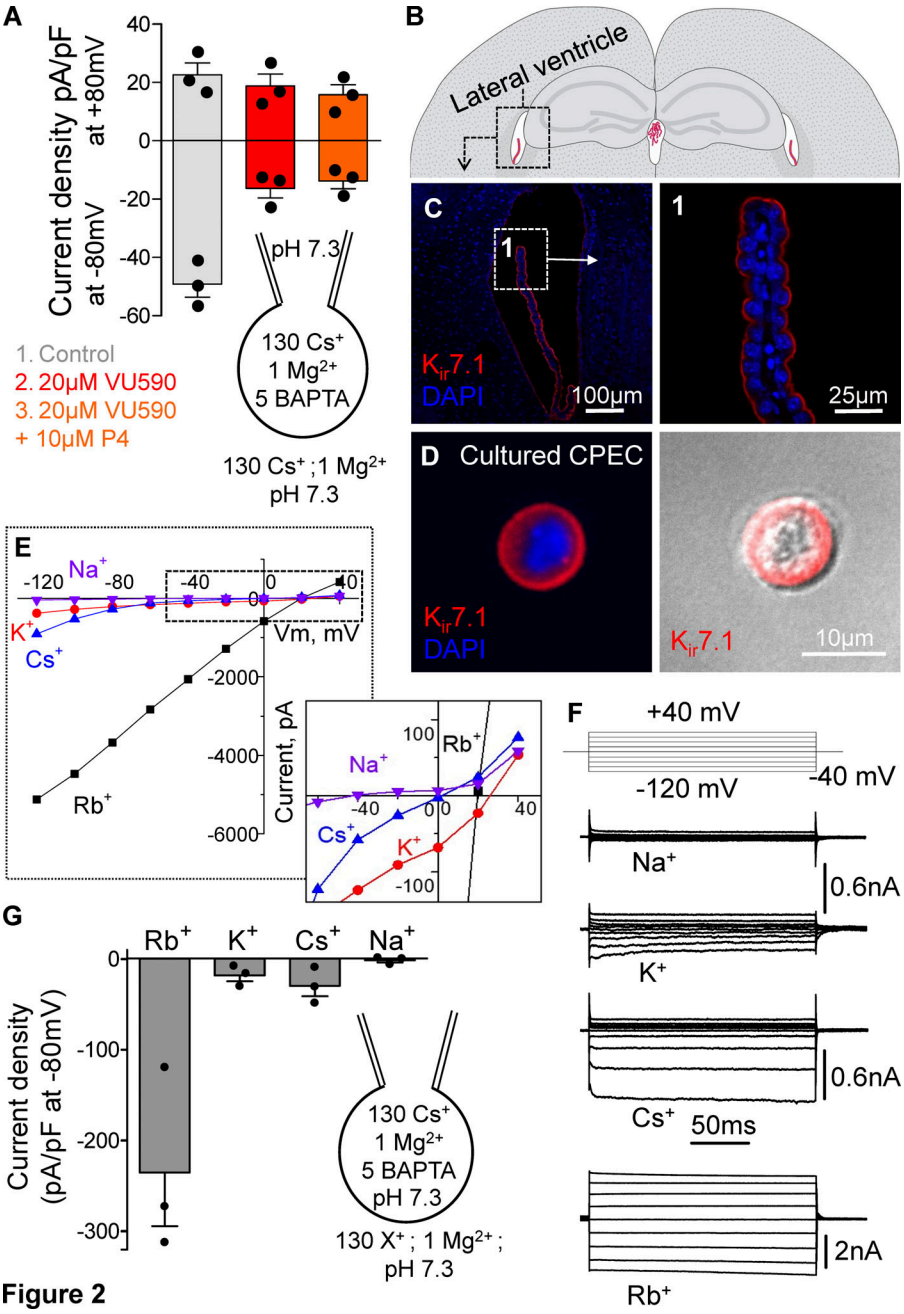

Figure 2

Figure 2. **Expression and permeability of Kir7.1 from murine CP. (A)** A reduction in current density was observed at −80 mV after applying 20 µM of the Kir7.1 and Kir1.1 inhibitor VU590 to CPECs. VU590 prevented any potentiation of the current by P4. **(B)** Schematic image showing localization of the lateral ventricle in the mouse brain. **(C)** Immunohistochemical image from a C57BL/6N adult male showing that Kir7.1 localized to the apical side of the lateral ventricle CP (1). **(D)** Kir7.1 is also detected in the plasma membrane of CPECs that have been isolated from an adult female mouse and cultured for 3 h. **(E and F)** Representative I-V relationships (E) extracted from representative traces (F) of Kir7.1 currents recorded in whole-cell mode from lateral CPECs in response to a voltage-step protocol (from −120 mV to +40 mV, in 20-mV increments, starting from a holding potential of −40 mV) as shown. Exposing CPECs to different bath solutions shows large conductance when the cells are in a Rb^+-based buffer, while Cs^+- and K^+-based buffers showed smaller but similar conductances. The Na^+-based bath solution did not elicit any current. Insert shows the shift in reverse potentials upon changes in the bath ion composition. **(G)** Current densities from three CPECs exposed to the different bath solutions at −80 mV, as recorded in E. Data are means ± SEM.

Furthermore, our mRNA-sequencing data provided evidence of a possible G protein–coupled progesterone receptor in the CP (Table 1), a signaling pathway previously shown to be involved in Kir7.1 regulation (Carrington et al., 2018). To test whether or not these signaling pathways would lead to the observed potentiation of Kir7.1 activation, 1 mM GDPβS, a competitive inhibitor of GTP activation of G-protein signaling, was applied to the pipette solution while recording Kir7.1 from either CPECs (Fig. 5, B and E) or HEK293 cells (Figs. 5 E and S3 A). In both cases, the presence of the inhibitor had no effect on P4- mediated Kir7.1 potentiation (Fig. 5, B and E), which further confirmed that G-protein signaling is not involved in P4 regulation of Kir7.1. It also must be mentioned that our intracellular (pipette) solutions did not contain ATP, GTP, or any other essential nucleotides required to power G-protein signaling. Recent reports suggest that Kir7.1 could be coupled to the melanocortin-4 receptor in a G protein–independent manner (Ghamari-Langroudi et al., 2015); however, melanocortin-4 receptor is not expressed in the murine CP (Data S1). Together, these results make a compelling argument for the activation of Kir7.1 to be caused by a direct interaction of steroid P4 with the channel.

Progesterone potentiates RPE Kir7.1 activity

Kir7.1 is also found in the RPE (Shimura et al., 2001), where the channel works in concert with the Na^+-K^+-ATPase to regulate K^+ homeostasis and photoreceptor excitability (Shahi et al., 2017). To determine if Kir7.1 in RPE cells shows similar activation by P4 as in CPECs, whole-cell patch-clamp recordings were performed.

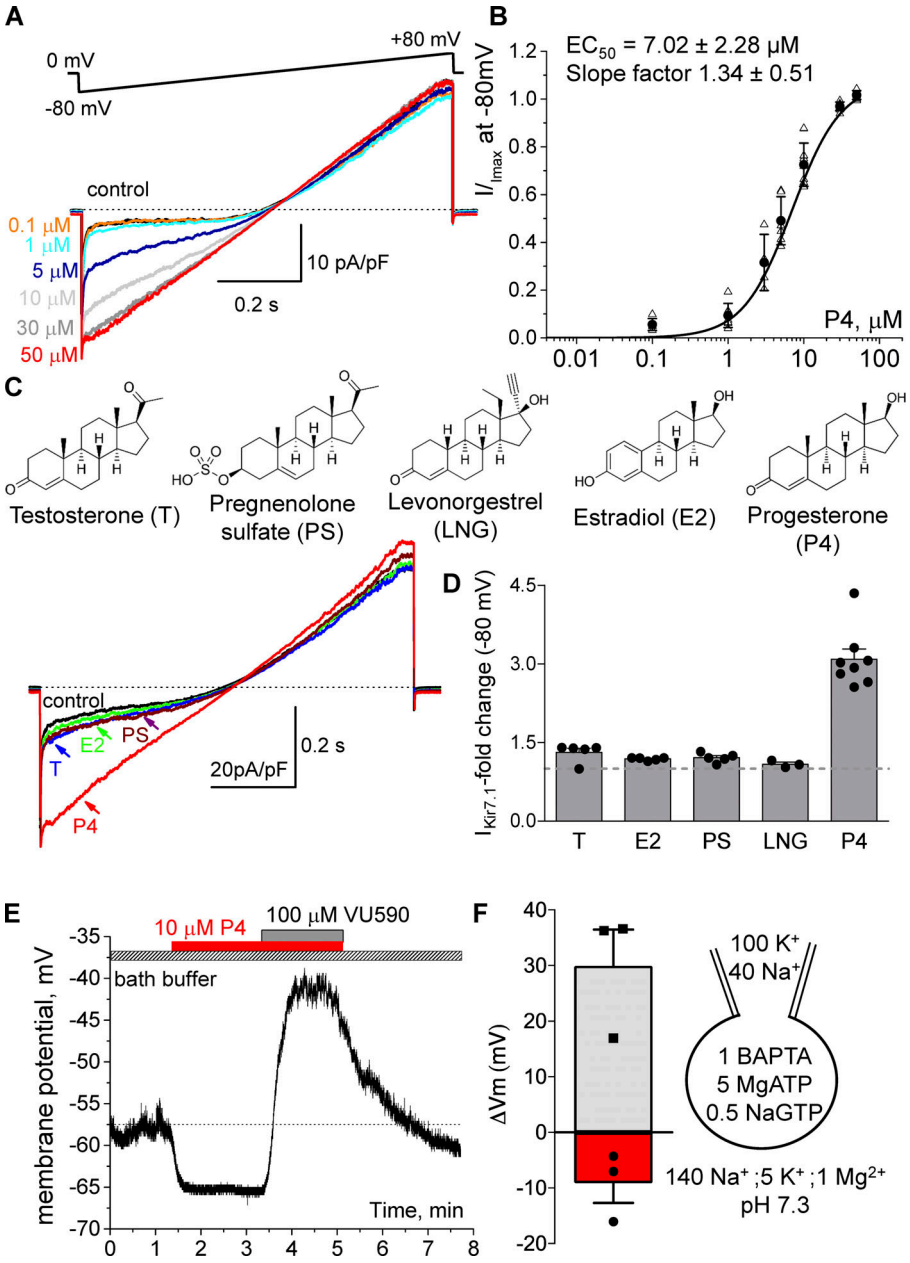

Figure 3. **Potentiation of Kir7.1 by steroid hormones. (A)** Representative traces recorded from female murine CPECs isolated from the lateral ventricle. A gradual increase in current was observed after applying increasing concentrations of P4 to the bath solution. **(B)** Half-maximal effective concentration (EC_{50}) for P4 was calculated using the average current density at −80 mV for 12 cells isolated from CPECs, as mentioned in A. **(C and D)** Representative traces (C) and the average current fold increase (D) of Kir7.1 at −80 mV recorded from five CPECs that were exposed to 10 μM testosterone (T), estradiol (E2), PS, and P4. Three CPEC were assessed on their modulation by 10 μM levonorgestrel (LNG). The chemical structure of the different steroids used for patch-clamp recordings is shown. The steroids were applied in different orders for each cell, with P4 always added last. **(E)** A representative current-clamp measurement, which shows hyperpolarization of a CPEC after applying 10 μM P4 (red) to the bath buffer. When blocking Kir7.1 activity with 100 μM VU590 a significant cellular depolarization was detected. **(F)** Average changes in membrane potential (mV) as measured by current-clamp recordings of three cells when applying 10 μM P4 (red bar, circles) or 100 μM VU590 + 10 μM P4 (gray bar, squares). Data are means ± SEM.

RPE cells that had been isolated and cultured overnight were used for the experiments (Fig. 6). The currents measured from these cells were considerably smaller than the currents of CPECs (Fig. 6, A–C; and Fig. S3 A), and the slow kinetics of the onset of P4 response as recorded from CPECs (Fig. 1 C) was absent from RPE recordings (Fig. 6 D). However, a statistically significant potentiation of inward $I_{Kir7.1}$ was observed after stimulation with 10 μM P4 (Figs. 6 C and S3 A). Thus, the effect of P4 on Kir7.1 activity is not limited to the CP but could, in addition, have important implications in other tissues.

Discussion

The adult murine CP represents a novel model to study nongenomic steroid signaling, because P4 is able to regulate this tissue (Lindvall-Axelsson and Owman, 1990; Kelley and Mermelstein, 2011) even under negligible expression levels of the nuclear progesterone receptor (Table 1 and Data S1). Since P4 is known to affect ion channels in neurons, either through a direct interaction between the steroid and the channel or through an indirect response that occurs following steroid binding to its receptor (Kelley and Mermelstein, 2011; Luoma et al., 2011; Majeed et al., 2011; Miehe et al., 2012; Miller et al., 2016), we aimed to determine whether P4 can influence ion conductance in CPECs via one of those mechanisms. By performing electrophysiological studies on CPECs, we showed a novel, P4-specific activation of an inwardly rectifying potassium channel, Kir7.1. This P4 activation was inhibited by the addition of VU590, a specific inhibitor of Kir1.1 and Kir7.1 channels. Since only Kir7.1 is highly expressed in CPECs, and all other potassium conductances were blocked by intracellular Cs ions, these experiments further confirm the channel identity. Furthermore,

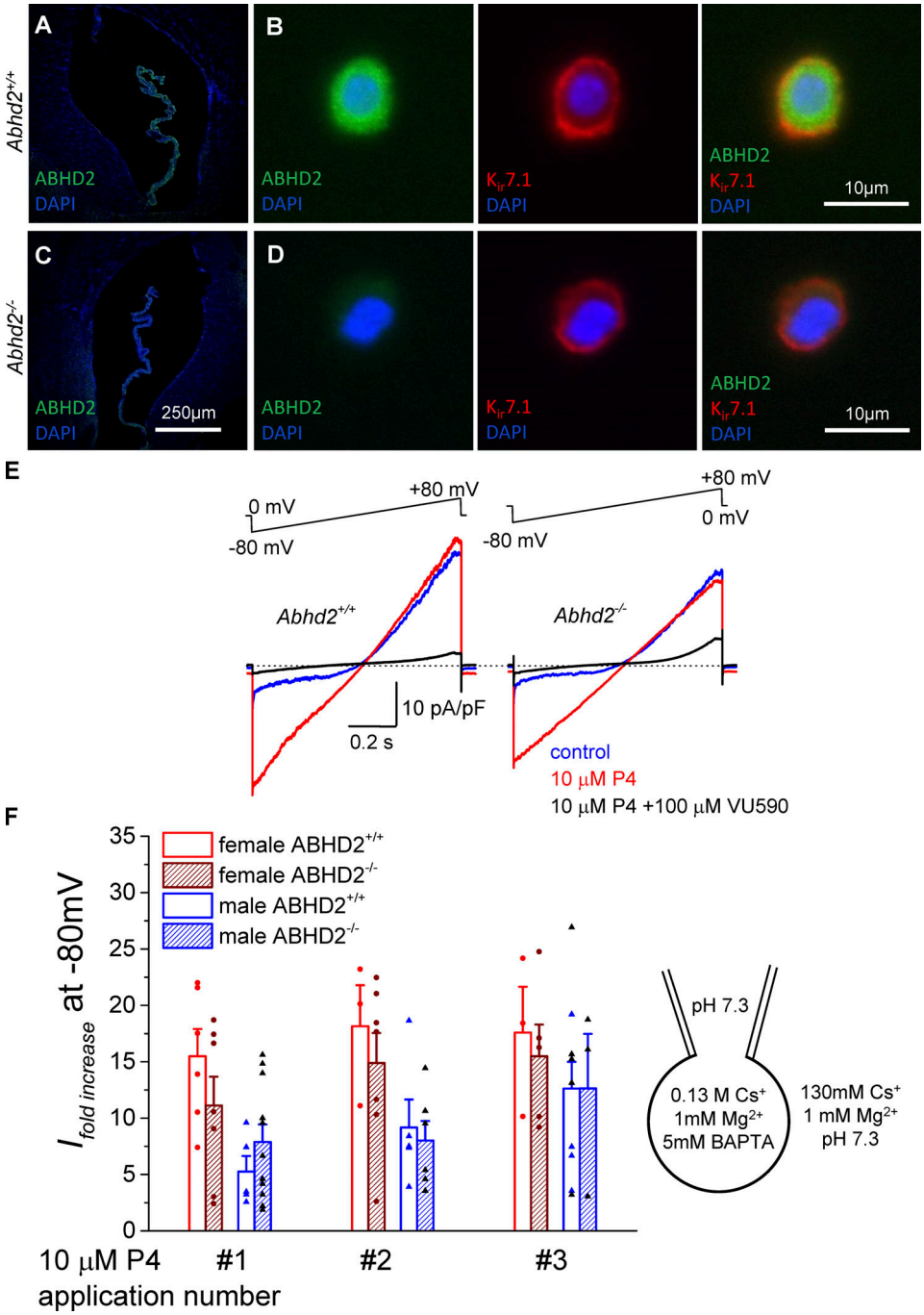

Figure 4. **Wild-type and *Abhd2*$^{-/-}$ murine CPECs show similar potentiation of Kir7.1 by progesterone (P4). (A and B)** Immunohistochemical staining of the lateral ventricle CP of ABHD2 in *Abhd2*$^{+/+}$ (A) and *Abhd2*$^{-/-}$ (B) adult male mice. **(C and D)** Immunocytochemical staining of cultured CPECs shows the presence of Kir7.1 in cells of both genotypes (*Abhd2*$^{+/+}$ and *Abhd2*$^{-/-}$), although the latter lack ABHD2. **(E)** Representative recordings from adult male CPECs from *Abhd2*$^{-/-}$ mice show potentiation of the Kir7.1 current similar to that of cells from *Abhd2*$^{+/+}$ animals when 10 μM P4 was added to the bath solution. Whole-cell recordings were performed using Cs^+ bath and pipette solutions, as indicated. **(F)** The fold change of $I_{Kir7.1}$ at −80 mV was calculated from recordings of 6 female and 10 male wild-type cells and 8 female and 16 male *Abhd2*$^{-/-}$ cells, as shown. Although the *Abhd2* knockout female cells show a slightly smaller current fold increase, the difference is not statistically significant when compared with that of wild-type cells.

the recorded conductance displayed Kir7.1-specific hallmarks, such as the lack of an internal Mg^{2+} block, a high Rb^+ conductivity, and a low sensitivity to Cs^+ (Krapivinsky et al., 1998; Shimura et al., 2001; Sackin et al., 2010). Eventually, we were able to recapitulate Kir7.1 potentiation by P4 with recombinantly expressed Kir7.1.

Interestingly, the potentiation of $I_{Kir7.1}$ by P4 was independent of ABHD2, a known P4 membrane receptor. This was confirmed by recordings from *Abhd2*-deficient murine CPECs, which retained a similar activation of Kir7.1 by P4. The involvement of G protein–coupled receptors in this process was ruled out, as addition of GDPβS, a competitive inhibitor of G-protein signaling,

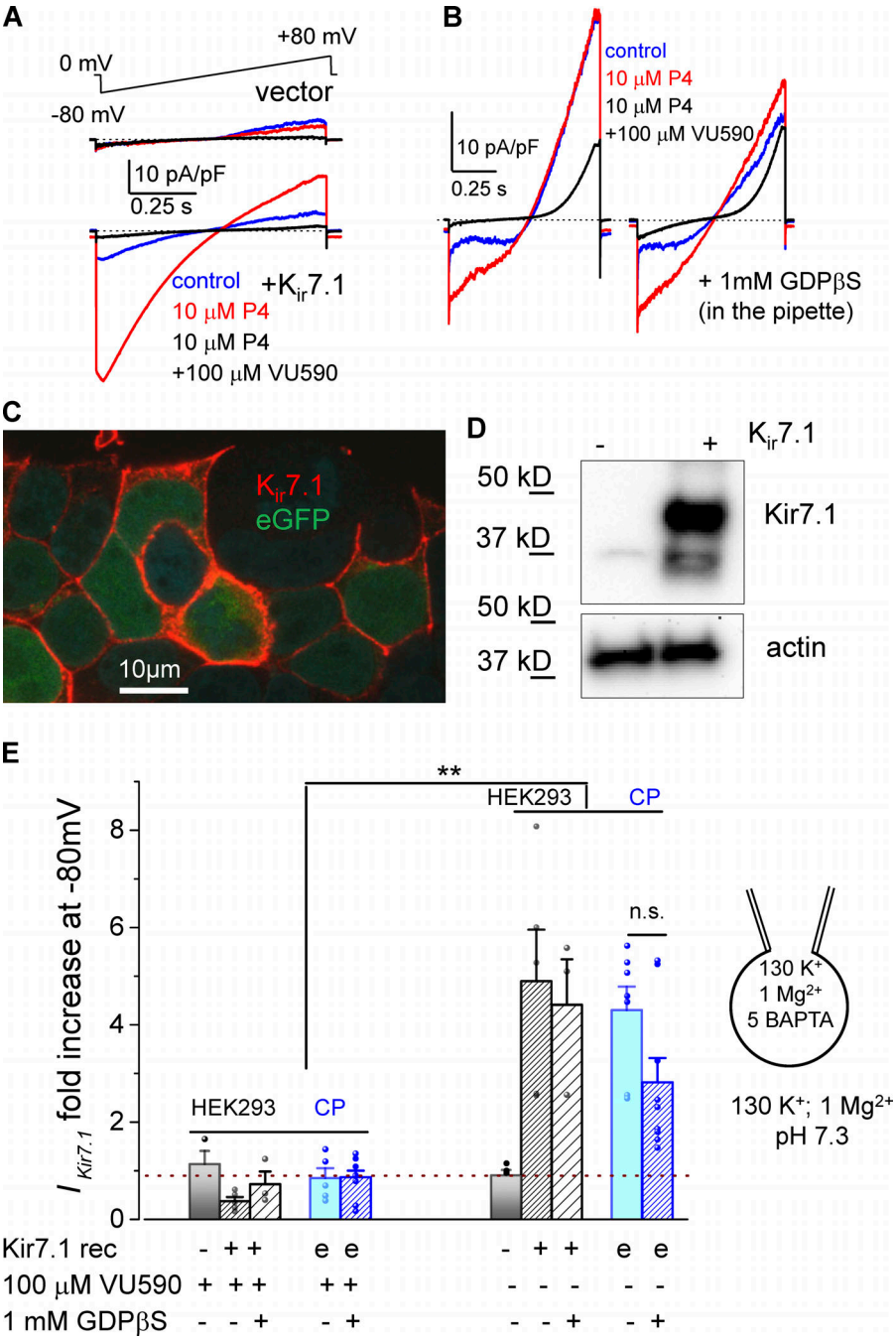

Figure 5. **Potentiation of Kir7.1 by progesterone in HEK293 and CPECs is independent of G protein–coupled receptor signaling.** **(A)** Representative traces recorded from HEK293 cells transfected with a pIRES2-EGFP/Kir7.1 construct show a fivefold potentiation of the current after addition of 10 μM P4 to the bath. The cells transfected with the empty vector (upper panel) do not respond to P4 or display $I_{Kir7.1}$. **(B)** Representative $I_{Kir7.1}$ from an isolated adult female lateral CPEC is similarly activated by 10 μM P4 in the presence of 1 mM GDPβS in the pipette. **(C)** Immunohistochemical staining of recombinant Kir7.1 in HEK293 cells transfected with the pIRES2-eGFP/Kir7.1 construct. **(D)** Western blotting detects both the mature glycosylated and the shorter immature product of Kir7.1 seen in HEK293 cells transfected with the pIRES2-EGFP/Kir7.1 construct. The cells transfected with the empty vector do not express Kir7.1. Actin was used as a loading control. **(E)** Graph depicting the fold change in the inward $I_{Kir7.1}$ after exposure to 10 μM P4 recorded from transfected HEK293 cells and CPECs, with "e" representing endogenous Kir7.1 expression as in CPECs. Statistical significance was calculated using the paired *t* test and the significance of changes is indicated as follows: **, P ≤ 0.01. Data are means ± SEM.

did not alter the potentiation of $I_{Kir7.1}$. Additionally, recordings of a recombinant Kir7.1 expressed in HEK293 cells, as well as recordings in the absence of intracellular messengers, such as GTP, displayed similar potentiation of Kir7.1 by P4. We, therefore, suggest that P4 activates Kir7.1 directly.

There were clear differences in stronger up-regulation of Kir7.1 by P4 recorded from female CPECs compared with those of age-matched male mice. Based on the gene expression profile (Table 2), *Kcnj13* expression is not statistically different between sexes; however, it is possible that a difference in the lipid composition of the plasma membranes of CP cells between males and females would be the cause of these distinct responses. This important phenomenon requires more in-depth studies to reveal the molecular basis behind the observed sex differences. Interestingly, previous studies on the effect of membrane fluidity on Kir channels have shown their sensitivity to cholesterol-driven regulation. Although the activity of most K_{ir} channels is suppressed with increased cholesterol levels in the membrane, Kir7.1 is an exception to the rule and, instead, showed a slight activation of ion flux (Rosenhouse-Dantsker et al., 2010). In silico analyses stated that this activation was caused by a weak interaction between Kir7.1 and cholesterol rather than a change in membrane fluidity (Fürst et al., 2014). Similarly, steroids are known to change the cell membrane fluidity (Whiting et al., 2000; McDonnel et al., 2003; Korkmaz and Severcan, 2005). If Kir7.1 activation by P4 was due only to an altered membrane

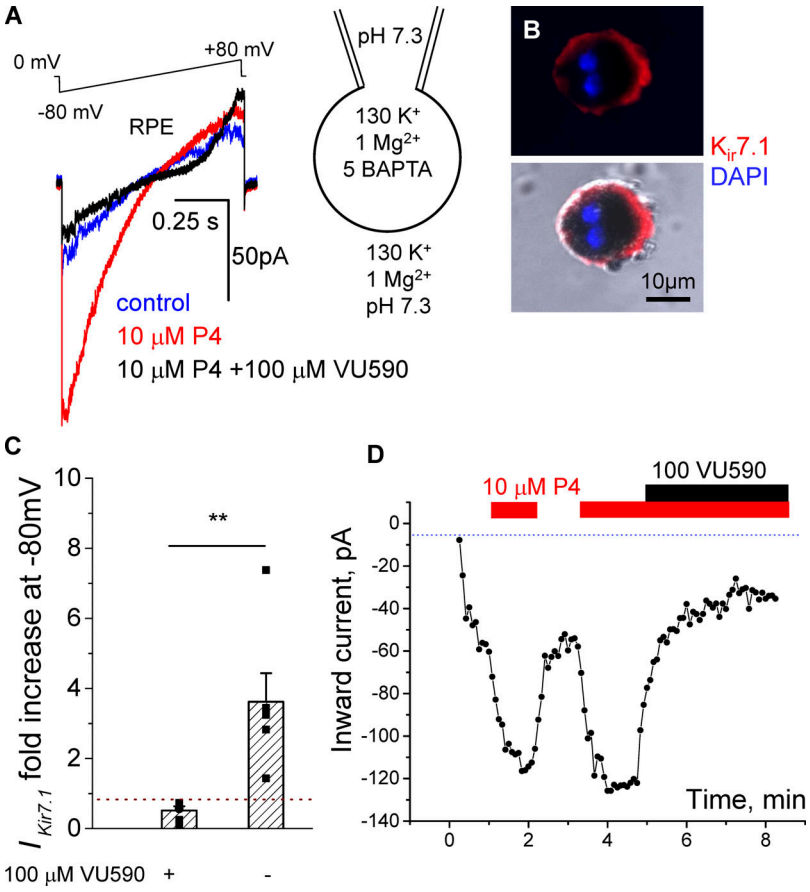

Figure 6. **Potentiation of Kir7.1 by progesterone in RPE cells. (A)** Representative whole-cell recordings from RPE cells in response to 10 μM P4. RPE was isolated from a 1-mo-old female mouse. A significant increase in the inward current density occurred at −80 mV, while the outward current recorded at +80 mV did not change. **(B)** Immunocytochemical staining of mouse RPE cells detects Kir7.1. **(C)** The fold change in the inward $I_{Kir7.1}$ after exposure to 10 μM P4 recorded from RPE cells. Statistical significance was calculated using the paired *t* test and the significance of changes is indicated as follows: **, P ≤ 0.01. Data are means ± SEM. **(D)** Representative inward current amplitudes obtained at −80 mV from the experiments shown in A and plotted against time show repetitive responses to P4 in female RPE cell. The time of applications of 10 μM P4 to the bath solution is indicated by red bars above. Addition of Kir7.1 inhibitor VU590 is shown by the black bar.

composition, then other lipophilic hormones would have had a similar effect on Kir7.1. However, none of the tested steroids (testosterone, estradiol, levonorgestrel, and PS) were able to influence $I_{Kir7.1}$. Thus, Kir7.1 displays a specific affinity for P4, and the mechanisms of such an interaction will be interesting to explore further. However, we cannot exclude the possibility that other steroid molecules can exhibit suppressing or inhibitory effect on Kir7.1 activity, and it is possible to assume that their basal concentration might be different in plasma membrane of the CP between sexes.

Another interesting observation is the slow kinetics of the onset of P4 responses that is only evident upon initial application of P4 to CP cells and is absent from consequent P4 applications or even the initial application of P4 to RPE cells. This could be explained by a presence of a still-unknown lipid factor, such as an inhibitory lipid, another steroid, or a potential additional Kir7.1 regulatory subunit, that must be eliminated or decoupled from the membrane or ion channel complex before P4 can exert its full effect. All of these important phenomena require follow-up studies that may shed a light on sex differences in CP physiology. As mentioned above, Kir7.1 is also found on the apical side of RPE cells, where it works in concert with the Na^+,K^+ pump to maintain the ion homeostasis of the subretinal space (Shimura et al., 2001). Kir7.1 is vital for normal RPE physiology, as RPE-specific deletion of the channel leads to photoreceptor degradation (Roman et al., 2018). Mutations in Kir7.1 gives rise to snowflake vitreoretinal degeneration and Leber congenital amaurosis, retinal dystrophy disorders that also cause blindness (Hejtmancik et al., 2008). Similar to CPECs, RPE cells use Kir7.1 to balance the ion content of the cell through secretion of K^+ ions taken up by the Na^+,K^+-ATPase. Our results showed that Kir7.1 expressed in RPE also responded to P4, which points to a potential regulatory role for P4 in the function of RPE. The effect of sex hormone signaling on RPE functions has not been well studied, although enzymes required for synthesis of P4 are found in the retina (Guarneri et al., 1994; Cascio et al., 2015). Changes in hormone production during aging are also thought to cause a difference in eye disorder prevalence among men and women (Cascio et al., 2015). Further studies on the connection between P4 production in the eye and Kir7.1 activity could give new insight into these discrepancies.

We are just beginning to observe the full impact of Kir7.1 on brain functions, especially since a recent study by Papanikolaou et al. (2019) showed expression of Kir7.1 throughout the brain in both neuronal and glial structures. Our data prompt future studies on the relationship between P4-driven Kir7.1 regulation and CSF production, as well as the regulation of ventricle size during brain trauma. It also would be important to explore the role of P4-activation of Kir7.1 in TBI pathology. At high enough concentrations, P4 could lead to hyperpolarization, altering ion exchange and inhibiting water secretion into the ventricles, which ultimately would benefit TBI patients. While the low micromolar concentration range required for Kir7.1 activation appears to be supraphysiological for CSF, which is known to

have a low composition of steroid carriers, the concentration of steroid hormones within the CPEC plasma membrane is not known. The filtration rate of the CP is ∼0.5 liters per day, which allows for a total exchange of the 150 ml CSF within the ventricular system three or four times daily (Marques et al., 2017). As filtration progresses, it leads to accumulation of lipophilic compounds and locally produced neurosteroids in the CPEC plasma membrane, which can ultimately reach the concentration levels required for channel modulation. The physiological concentrations of P4 in CSF fluctuate between 0.1 nM (Datta et al., 1986) and 10 nM (Datta et al., 1986; during pregnancy); however, circulating P4 concentrations can reach high micromolar concentrations upon intramuscular or intravenous injections of 1–80 mg P4 during the course of TBI treatment (Pan et al., 2019), which potentially could lead to Kir7.1 modulation.

CP represents a convenient tissue to study the physiology of ion channels, particularly their regulation by steroid hormones via nongenomic mechanisms (Haoui et al., 2021), because of the low expression of genomic steroid receptors in the adult CP (Table 1). As is evident from CP gene expression analyses (Data S1), several transient receptor potential ion channels, such as TRPM3 and TRPV4, were also found to be expressed in CP (Millar et al., 2007). In fact, TRPM3 regulation by PS (Majeed et al., 2012) can be recorded from CP cells upon inhibition of Kir7.1 activity by VU590 (Fig. S3 B). Additionally, TRPM3 conductance could be partially responsible for the outward currents that were observed in this study.

In conclusion, the inwardly rectifying potassium channel Kir7.1 is emerging as the major ion channel in the CP potentiated by P4 via a G protein–coupled receptor-independent mechanism. As few endogenous regulators of Kir7.1 are known, its P4 activation represents a novel significant regulatory modality for this channel. The potentiation of Kir7.1 by P4 was steroid specific and took place regardless of what cell type the channel was expressed in. The impact of P4 regulation on Kir7.1 may, therefore, not be limited to the CP and RPE but extend to all tissues where the channel is found. Future studies should focus on the possible impact of increased P4 levels on these tissues.

Acknowledgments

Joseph A. Mindell served as editor.

We thank Dr. Xiaoquan Li for help with the pilot experiments involving in situ staining for ABHD2, Dr. Terry Machen for help with equipment and advice on epithelial biology, Elena Solonenko for help with cell preparations, and Dr. Lin He laboratory for advice on initial isolation of the CP.

This work was supported by National Institutes of Health grant R01GM111802, a Pew Innovation Fund 2020 award from Pew Charitable Trusts, a Rose Hills Foundation award, and Packer Wentz Endowment Will. This work was also funded in part by the Global Consortium for Reproductive Longevity and Equality at the Buck Institute, made possible by the Bia-Echo Foundation, award GCRLE-0920 (P.V. Lishko). This work also used the Vincent J. Coates Genomics Sequencing Laboratory at University of California, Berkeley, which is supported by National Institutes of Health instrumentation grant S10 OD018174.

The authors declare no competing financial interests.

Author contributions: I. Björkgren and P.V. Lishko contributed to the conception and design of this research and wrote the manuscript together with M. Haoui. All authors performed experiments, analyzed data, and reviewed and approved the final version of the manuscript.

Submitted: 2 April 2021
Accepted: 29 July 2021

References

Björkgren, I., S. Mendoza, L. Gabelev-Khasin, A. Modzelewski, L. He, and P.V. Lishko. 2019. Alpha/Beta Hydrolase Domain-Containing Protein 2 regulates the rhythm of follicular maturation and estrous stages of the female reproductive cycle. *bioRxiv*. https://doi.org/10.1101/684951 (Preprint posted July 2, 2019)

Carrington, S.J., C.C. Hernandez, D.R. Swale, O.A. Aluko, J.S. Denton, and R.D. Cone. 2018. G protein-coupled receptors differentially regulate glycosylation and activity of the inwardly rectifying potassium channel Kir7.1. *J. Biol. Chem.* 293:17739–17753. https://doi.org/10.1074/jbc.RA118.003238

Cascio, C., I. Deidda, D. Russo, and P. Guarneri. 2015. The estrogenic retina: The potential contribution to healthy aging and age-related neurodegenerative diseases of the retina. *Steroids*. 103:31–41. https://doi.org/10.1016/j.steroids.2015.08.002

Damkier, H.H., P.D. Brown, and J. Praetorius. 2013. Cerebrospinal fluid secretion by the choroid plexus. *Physiol. Rev.* 93:1847–1892. https://doi.org/10.1152/physrev.00004.2013

Datta, S., R.J. Hurley, J.S. Naulty, P. Stern, D.H. Lambert, M. Concepcion, D. Tulchinsky, J.B. Weiss, and G.W. Ostheimer. 1986. Plasma and cerebrospinal fluid progesterone concentrations in pregnant and nonpregnant women. *Anesth. Analg.* 65:950–954. https://doi.org/10.1213/00000539-198609000-00007

Deutsch, E.R., T.R. Espinoza, F. Atif, E. Woodall, J. Kaylor, and D.W. Wright. 2013. Progesterone's role in neuroprotection, a review of the evidence. *Brain Res.* 1530:82–105. https://doi.org/10.1016/j.brainres.2013.07.014

Edgar, R., M. Domrachev, and A.E. Lash. 2002. Gene Expression Omnibus: NCBI gene expression and hybridization array data repository. *Nucleic Acids Res.* 30:207–210. https://doi.org/10.1093/nar/30.1.207

Fürst, O., C.G. Nichols, G. Lamoureux, and N. D'Avanzo. 2014. Identification of a cholesterol-binding pocket in inward rectifier K(+; Kir) channels. *Biophys. J.* 107:2786–2796. https://doi.org/10.1016/j.bpj.2014.10.066

Ghamari-Langroudi, M., G.J. Digby, J.A. Sebag, G.L. Millhauser, R. Palomino, R. Matthews, T. Gillyard, B.L. Panaro, I.R. Tough, H.M. Cox, et al. 2015. G-protein-independent coupling of MC4R to Kir7.1 in hypothalamic neurons. *Nature*. 520:94–98. https://doi.org/10.1038/nature14051

Guarneri, P., R. Guarneri, C. Cascio, P. Pavasant, F. Piccoli, and V. Papadopoulos. 1994. Neurosteroidogenesis in rat retinas. *J. Neurochem.* 63:86–96. https://doi.org/10.1046/j.1471-4159.1994.63010086.x

Hagemann, G., T. Ugur, E. Schleussner, H.J. Mentzel, C. Fitzek, O.W. Witte, and C. Gaser. 2011. Changes in brain size during the menstrual cycle. *PLoS One*. 6:e14655. https://doi.org/10.1371/journal.pone.0014655

Haoui, M., N.T. Petersen, I. Björkgren, D.H. Chung, and P.V. Lishko. 2021. Choroid plexus epithelial cells as a model to study nongenomic steroid signaling and its effect on ion channel function. *Methods Enzymol.* 654:297–314. https://doi.org/10.1016/bs.mie.2021.03.004

Hejtmancik, J.F., X. Jiao, A. Li, Y.V. Sergeev, X. Ding, A.K. Sharma, C.C. Chan, I. Medina, and A.O. Edwards. 2008. Mutations in KCNJ13 cause autosomal-dominant snowflake vitreoretinal degeneration. *Am. J. Hum. Genet.* 82:174–180. https://doi.org/10.1016/j.ajhg.2007.08.002

Ishii, T., M. Omura, and P. Mombaerts. 2004. Protocols for two- and three-color fluorescent RNA in situ hybridization of the main and accessory olfactory epithelia in mouse. *J. Neurocytol.* 33:657–669. https://doi.org/10.1007/s11068-005-3334-y

Kelley, B.G., and P.G. Mermelstein. 2011. Progesterone blocks multiple routes of ion flux. *Mol. Cell. Neurosci.* 48:137–141. https://doi.org/10.1016/j.mcn.2011.07.002

Korkmaz, F., and F. Severcan. 2005. Effect of progesterone on DPPC membrane: evidence for lateral phase separation and inverse action in lipid dynamics. *Arch. Biochem. Biophys.* 440:141–147. https://doi.org/10.1016/j.abb.2005.06.013

Krapivinsky, G., I. Medina, L. Eng, L. Krapivinsky, Y. Yang, and D.E. Clapham. 1998. A novel inward rectifier K+ channel with unique pore properties. *Neuron.* 20:995–1005. https://doi.org/10.1016/S0896-6273(00)80480-8

Lindvall-Axelsson, M., and C. Owman. 1990. Actions of sex steroids and corticosteroids on rabbit choroid plexus as shown by changes in transport capacity and rate of cerebrospinal fluid formation. *Neurol. Res.* 12:181–186. https://doi.org/10.1080/01616412.1990.11739940

Lösel, R., and M. Wehling. 2003. Nongenomic actions of steroid hormones. *Nat. Rev. Mol. Cell Biol.* 4:46–56. https://doi.org/10.1038/nrm1009

Lun, M.P., E.S. Monuki, and M.K. Lehtinen. 2015. Development and functions of the choroid plexus-cerebrospinal fluid system. *Nat. Rev. Neurosci.* 16: 445–457. https://doi.org/10.1038/nrn3921

Luoma, J.I., B.G. Kelley, and P.G. Mermelstein. 2011. Progesterone inhibition of voltage-gated calcium channels is a potential neuroprotective mechanism against excitotoxicity. *Steroids.* 76:845–855. https://doi.org/10.1016/j.steroids.2011.02.013

Majeed, Y., M.S. Amer, A.K. Agarwal, L. McKeown, K.E. Porter, D.J. O'Regan, J. Naylor, C.W. Fishwick, K. Muraki, and D.J. Beech. 2011. Stereoselective inhibition of transient receptor potential TRPC5 cation channels by neuroactive steroids. *Br. J. Pharmacol.* 162:1509–1520. https://doi.org/10.1111/j.1476-5381.2010.01136.x

Majeed, Y., S. Tumova, B.L. Green, V.A. Seymour, D.M. Woods, A.K. Agarwal, J. Naylor, S. Jiang, H.M. Picton, K.E. Porter, et al. 2012. Pregnenolone sulphate-independent inhibition of TRPM3 channels by progesterone. *Cell Calcium.* 51:1–11. https://doi.org/10.1016/j.ceca.2011.09.005

Marques, F., J.C. Sousa, M.A. Brito, J. Pahnke, C. Santos, M. Correia-Neves, and J.A. Palha. 2017. The choroid plexus in health and in disease: dialogues into and out of the brain. *Neurobiol. Dis.* 107:32–40. https://doi.org/10.1016/j.nbd.2016.08.011

McDonnel, A.C., E.A. Van Kirk, D.D. Isaak, and W.J. Murdoch. 2003. Inhibitory effects of progesterone on plasma membrane fluidity and tumorigenic potential of ovarian epithelial cancer cells. *Exp. Biol. Med. (Maywood).* 228:308–314. https://doi.org/10.1177/153537020322800310

Miehe, S., P. Crause, T. Schmidt, M. Löhn, H.W. Kleemann, T. Licher, W. Dittrich, H. Rütten, and C. Strübing. 2012. Inhibition of diacylglycerol-sensitive TRPC channels by synthetic and natural steroids. *PLoS One.* 7: e35393. https://doi.org/10.1371/journal.pone.0035393

Millar, I.D., J.Ie. Bruce, and P.D. Brown. 2007. Ion channel diversity, channel expression and function in the choroid plexuses. *Cerebrospinal Fluid Res.* 4:8. https://doi.org/10.1186/1743-8454-4-8

Miller, M.R., N. Mannowetz, A.T. Iavarone, R. Safavi, E.O. Gracheva, J.F. Smith, R.Z. Hill, D.M. Bautista, Y. Kirichok, and P.V. Lishko. 2016. Unconventional endocannabinoid signaling governs sperm activation via the sex hormone progesterone. *Science.* 352:555–559. https://doi.org/10.1126/science.aad6887

Mortazavi, A., B.A. Williams, K. McCue, L. Schaeffer, and B. Wold. 2008. Mapping and quantifying mammalian transcriptomes by RNA-Seq. *Nat. Methods.* 5:621–628. https://doi.org/10.1038/nmeth.1226

Oatridge, A., A. Holdcroft, N. Saeed, J.V. Hajnal, B.K. Puri, L. Fusi, and G.M. Bydder. 2002. Change in brain size during and after pregnancy: study in healthy women and women with preeclampsia. *AJNR Am. J. Neuroradiol.* 23:19–26.

Pan, Z.Y., Y.H. Zhao, W.H. Huang, Z.Z. Xiao, and Z.Q. Li. 2019. Effect of progesterone administration on the prognosis of patients with severe traumatic brain injury: a meta-analysis of randomized clinical trials. *Drug Des. Devel. Ther.* 13:265–273. https://doi.org/10.2147/DDDT.S192633

Papanikolaou, M., A. Lewis, and A.M. Butt. 2019. Glial and neuronal expression of the Inward Rectifying Potassium Channel Kir7.1 in the adult mouse brain. *J. Anat.* 235:984–996. https://doi.org/10.1111/joa.13048

Pettus, E.H., D.W. Wright, D.G. Stein, and S.W. Hoffman. 2005. Progesterone treatment inhibits the inflammatory agents that accompany traumatic brain injury. *Brain Res.* 1049:112–119. https://doi.org/10.1016/j.brainres.2005.05.004

Roman, D., H. Zhong, S. Yaklichkin, R. Chen, and G. Mardon. 2018. Conditional loss of Kcnj13 in the retinal pigment epithelium causes photoreceptor degeneration. *Exp. Eye Res.* 176:219–226. https://doi.org/10.1016/j.exer.2018.07.014

Rosenhouse-Dantsker, A., E. Leal-Pinto, D.E. Logothetis, and I. Levitan. 2010. Comparative analysis of cholesterol sensitivity of Kir channels: role of the CD loop. *Channels (Austin).* 4:63–66. https://doi.org/10.4161/chan.4.1.10366

Sackin, H., M. Nanazashvili, H. Li, L.G. Palmer, and D.E. Walters. 2010. A conserved arginine near the filter of Kir1.1 controls Rb/K selectivity. *Channels (Austin).* 4:203–214. https://doi.org/10.4161/chan.4.3.11982

Shahi, P.K., X. Liu, B. Aul, A. Moyer, A. Pattnaik, J. Denton, D.M. Pillers, and B.R. Pattnaik. 2017. Abnormal Electroretinogram after Kir7.1 Channel Suppression Suggests Role in Retinal Electrophysiology. *Sci. Rep.* 7: 10651. https://doi.org/10.1038/s41598-017-11034-1

Shimura, M., Y. Yuan, J.T. Chang, S. Zhang, P.A. Campochiaro, D.J. Zack, and B.A. Hughes. 2001. Expression and permeation properties of the K(+) channel Kir7.1 in the retinal pigment epithelium. *J. Physiol.* 531:329–346. https://doi.org/10.1111/j.1469-7793.2001.0329i.x

Stein, D.G., and D.W. Wright. 2010. Progesterone in the clinical treatment of acute traumatic brain injury. *Expert Opin. Investig. Drugs.* 19:847–857. https://doi.org/10.1517/13543784.2010.489549

Whiting, K.P., C.J. Restall, and P.F. Brain. 2000. Steroid hormone-induced effects on membrane fluidity and their potential roles in non-genomic mechanisms. *Life Sci.* 67:743–757. https://doi.org/10.1016/S0024-3205(00)00669-X

Yin, W., H.T. Kim, S. Wang, F. Gunawan, L. Wang, K. Kishimoto, H. Zhong, D. Roman, J. Preussner, S. Guenther, et al. 2018. The potassium channel KCNJ13 is essential for smooth muscle cytoskeletal organization during mouse tracheal tubulogenesis. *Nat. Commun.* 9:2815. https://doi.org/10.1038/s41467-018-05043-5

Supplemental material

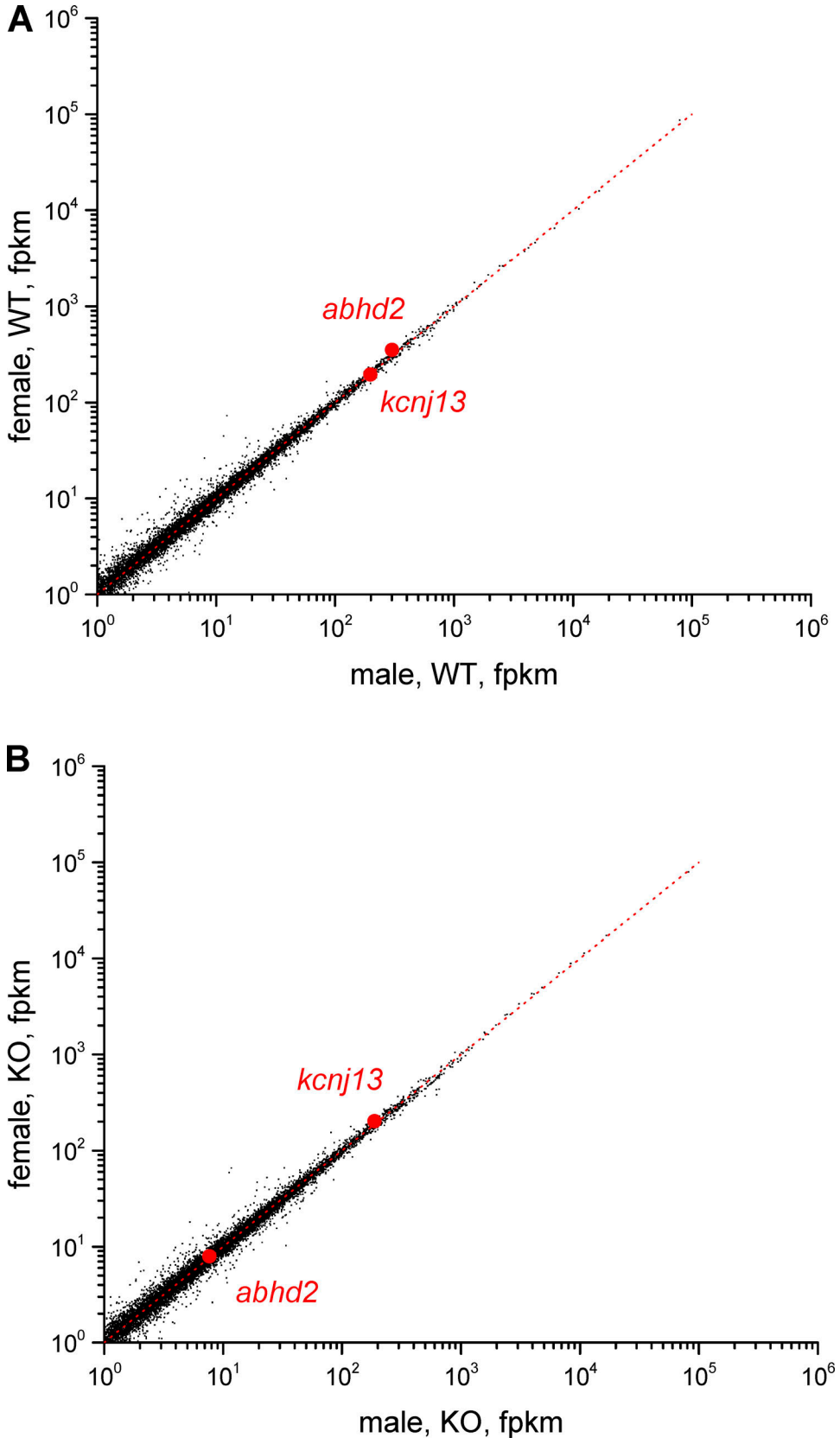

Figure S1. **The relative gene expression of the lateral CPs isolated from *Abhd2*$^{+/+}$ and *Abhd2*$^{-/-}$ male and female mice.** Number of mRNA-sequencing reads from corresponding CPs mapped to the mouse genome. *Abhd2* and *Kcnj13* expression levels are shown for wild-type (A) and knockout (B). Red dotted lines represent an expected number of sequencing reads for genes with similar expression levels between two samples. Signals <10 reads are within statistical noise and therefore scored as nonexpressed sequences. Data are averaged from triplicate experiments for each genotype and sex.

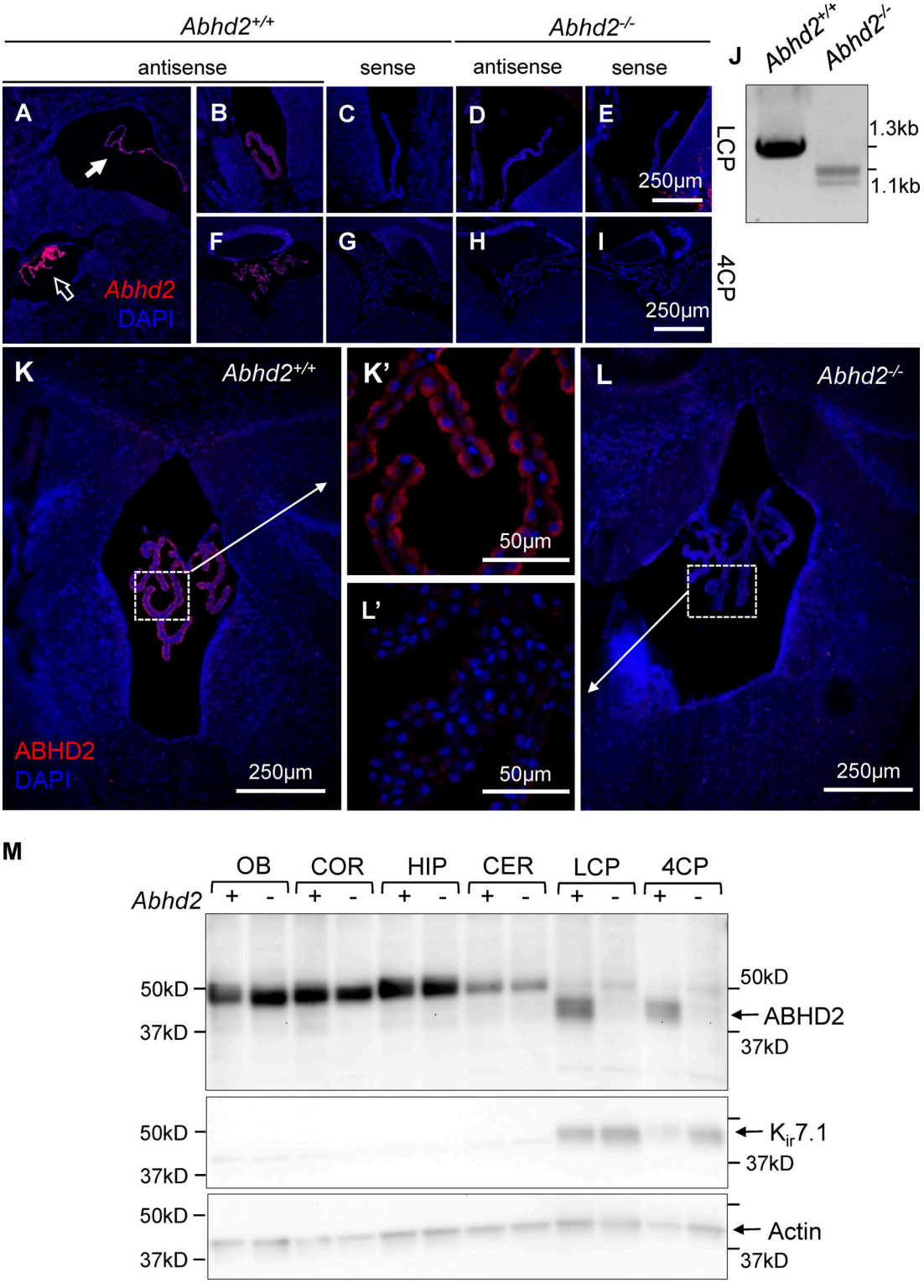

Figure S2. **Expression of *Abhd2* in murine CPs. (A, B, and F)** ISH shows strong expression of *Abhd2* in the lateral (A, solid arrow; and B), third (A, open arrow), and fourth ventricle CP (F) of *Abhd2*$^{+/+}$ mice. **(D, E, H, and I)** The adult *Abhd2*$^{-/-}$ mice display similar background staining when using either the antisense (D and H) or the sense (E and I) probe against *Abhd2*. **(J)** Although the antisense probe failed to bind to *Abhd2* mRNA in the *Abhd2*$^{-/-}$ animals in ISH experiments, a product lacking either *Abhd2* exon 6 or both exon 6 and exon 7 was detected in the kidney of *Abhd2*$^{-/-}$ mice. However, this mRNA product would lead to a frameshift and results in a truncated nonfunctional form of the protein. **(K, K', and M)** ABHD2 protein was detected by immunohistochemistry and Western blot in the CP of *Abhd2*$^{+/+}$ mice (K and M), with a localization on the apical side of the epithelium (K'). **(L and L')** ABHD2 was not detected in CP of *Abhd2*$^{-/-}$ mice (L'). **(M)** ABHD2 was not detected in the other regions of the brain, such as the olfactory bulb (OB), cortex (COR), hippocampus (HIP), and cerebellum (CER). However, it was exclusively found in both the lateral (LCP) and the fourth (4CP) ventricle CP of *Abhd2*$^{+/+}$ animals. *Abhd2*$^{-/-}$ animals display a strong expression of Kir7.1 even in the absence of ABHD2. Actin was used as a loading control.

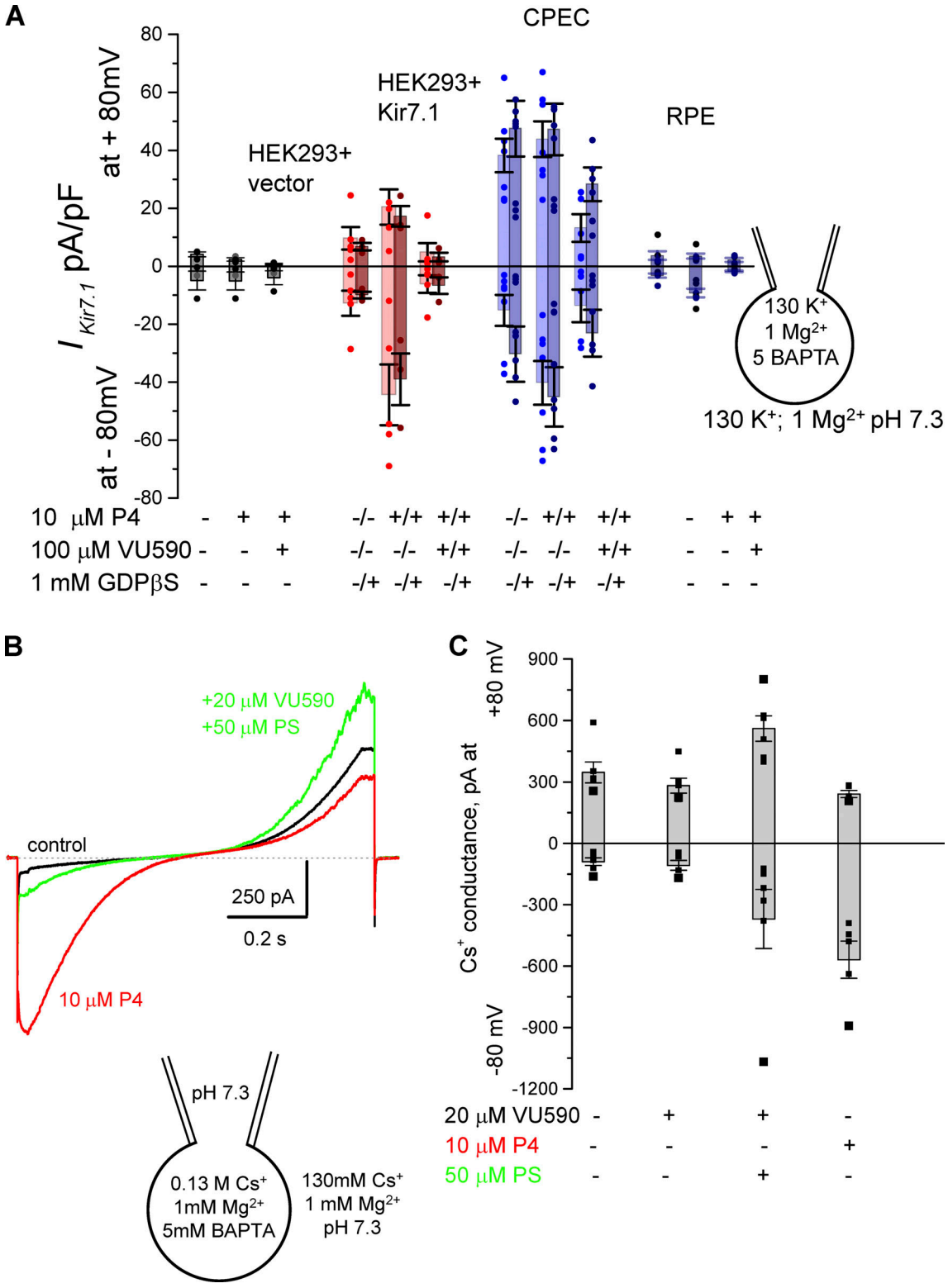

Figure S3. **Cumulative current densities of recordings from HEK293, RPE, and CP cells. (A)** Cumulative current densities recorded at −80 mV and +80 mV for all recordings shown in this study. Data are means ± SEM. Current densities recorded from HEK293 cells transfected with a recombinant Kir7.1 or with the empty vector, as well as from CPECs and RPE cells. Currents were recorded in the presence or absence of P4, GDPβS, or VU590 as indicated. HEK293 cells transfected with the empty vector were used as a control. **(B)** Whole-cell recordings from CPECs depict the presence of two ion channels, Kir7.1 and TRPM3. Representative traces from CPECs elicited in response to a voltage ramp from −80 mV to +80 mV from a holding potential of 0 mV. Under the condition where Kir7.1 activity is inhibited by 20 μM VU590, an additional conductance can be stimulated by an application of 50 μM PS (green), a TRPM3 channel agonist. Application of 10 μM P4 (red) in the absence of VU590 and PS results in Kir7.1 activation on the same CPEC. **(C)** Cumulative current densities recorded at −80 mV and +80 mV in the control condition, in the presence of VU590 and/or PS or P4. Data are means ± SEM.

Data S1 is provided online as a separate Excel file and shows the gene expression profile of the lateral CPs from wild-type and *Abhd2*$^{-/-}$ male and female mice.